Supporting Information

Boosting the Performance of MA-free Inverted Perovskite Solar Cells via Multifunctional Ion Liquid

Dongyang Li[a,b], Yulan Huang[b], Guoliang Wang[b], Qing Lian[b], Run Shi[b], Luozheng Zhang[b], Xingfu Wang[a], Fangliang Gao[a], Weiguang Kong[d,e,], Baomin Xu[b], Chun Cheng[b,c*] and Shuti Li[a,*]*

a Guangdong Engineering Research Center of Optoelectronic Functional Materials and Devices, South China Normal University, Guangzhou, 510631, China.

b Department of Materials Science and Engineering, Southern University of Science and Technology (SUSTech), Shenzhen, 518055, China.

c Key Laboratory of Energy Conversion and Storage Technologies (Southern University of Science and Technology), Ministry of Education, Shenzhen 518055, China.

d Hebei Key Laboratory of Optic-electronic Information and Materials and National-Local Joint Engineering Laboratory of New Energy Photoelectric Devices, College of Physics Science and Technology, Hebei University, Baoding, 071002, China.

e State Key Laboratory of Photovoltaic Materials & Technology, Yingli Solar, Baoding, 071051, China.

Corresponding Authors: kongwg@hbu.edu.cn (W.K.); chengc@sustech.edu.cn (C.C.); lishuti@scnu.edu.cn (S.L.)

Table S1. Recent development on MA-free inverted perovskite solar cells

Perovskite	Structure	Voc	Jsc	FF	PCE	Stability
$Cs_{0.05}FA_{0.95}PbI_3$ (bandgap ~1.5 eV)	ITO/PTAA/PFN-P_2/perovskite/LiF/C_{60}/BCP/Cu	**1.05**	**25.1**	**0.75**	**19.8**[1]	N/A
$Cs_{0.03}FA_{0.97}PbI_3$ (bandgap ~1.5 eV)	ITO/PTAA/perovskite/ PCBM/C_{60}/BCP/Ag	**1.06**	**24.7**	**0.72**	**18.2**[2]	N/A
$Cs_{0.06}FA_{0.94}PbI_3$ (bandgap ~1.5 eV)	ITO/PTAA/perovskite/ PCBM/AZO/SnO_2/Ag	**1.07**	**23.1**	**0.75**	**18.5**[3]	N/A
$Cs_{0.15}FA_{0.85}PbI_{2.7}Br_{0.3}$ (bandgap ~1.58 eV)	ITO/NiOx/$CuGaO_2$/perovskite/ PCBM/BCP/Ag	**1.11**	**23.19**	**0.80**	**20.7**[4]	85% under 85℃ 1000h
$Cs_{0.15}FA_{0.85}PbI_{2.85}Br_{0.15}$ (bandgap ~1.56 eV)	ITO/NiMgLiO/perovskite/ PCBM/BCP/Ag	**1.08**	**23.23**	**0.80**	**20.0**[5]	90% under 85℃ 500h
$Cs_{0.15}FA_{0.85}PbI_{2.7}Br_{0.3}$ (bandgap ~1.58 eV)	ITO/PTAA/PFN-P_2/perovskite/LiF/C_{60}/BCP/Cu	**1.10**	**22.92**	**0.81**	**20.3**[6]	80% under MPP 230h
$Cs_{0.17}FA_{0.83}PbI_{2.4}Br_{0.6}$ (bandgap ~1.61 eV)	ITO/PTAA/PFN-Br/perovskite/ bFPI/C_{60}/BCP/Cu	**1.15**	**22.58**	**0.81**	**21.1**[7]	91% under 85℃ 500h
$Cs_{0.17}FA_{0.83}Pb(I_{1-x}Br_x)_3$ (bandgap ~1.66 eV)	ITO/Poly-TPD /perovskite/PCBM/BCP/Cr/Au	**1.12**	**22.8**	**0.79**	**20.1**[8]	80% under 60℃1010h
$Cs_{0.15}FA_{0.85}PbI_3$ (bandgap ~1.54 eV)	ITO/NiOx/perovskite/PCBM/ BCP/Cu	**1.10**	**23.54**	**0.80**	**20.7**[9]	95% under 1000h
$Cs_{0.05}FA_{0.95}PbI_3$ (bandgap ~1.53 eV)	ITO/PTAA/perovskite/C_{60}/BCP/C u	**1.09**	**23.54**	**0.83**	**21.25**	94% under 85℃ 500h (This work)

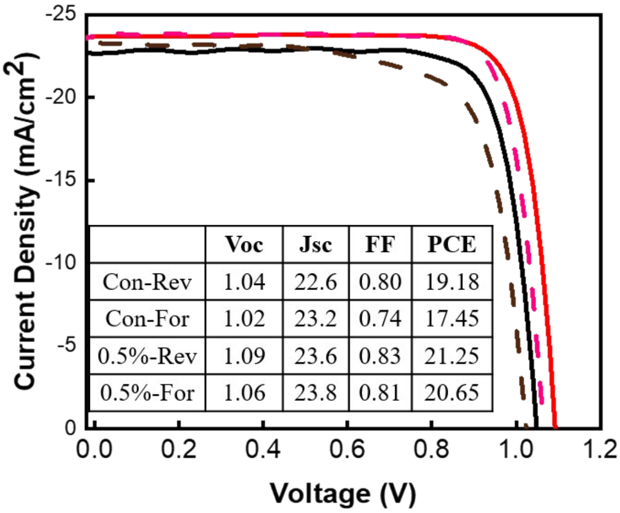

	Voc	Jsc	FF	PCE
Con-Rev	1.04	22.6	0.80	19.18
Con-For	1.02	23.2	0.74	17.45
0.5%-Rev	1.09	23.6	0.83	21.25
0.5%-For	1.06	23.8	0.81	20.65

Figure S1 Forward-Reverse Scan of PSCs

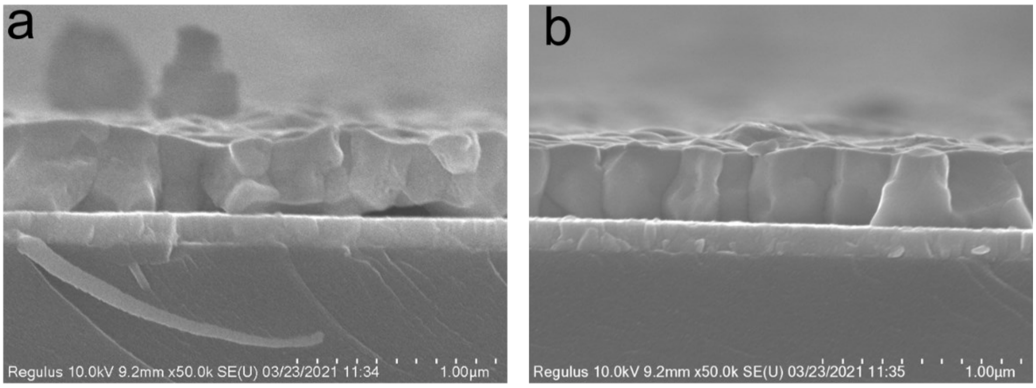

Figure S2 Cross-sectional SEM for control (a) and 0.5% NDAPBF4 (b) perovskite film

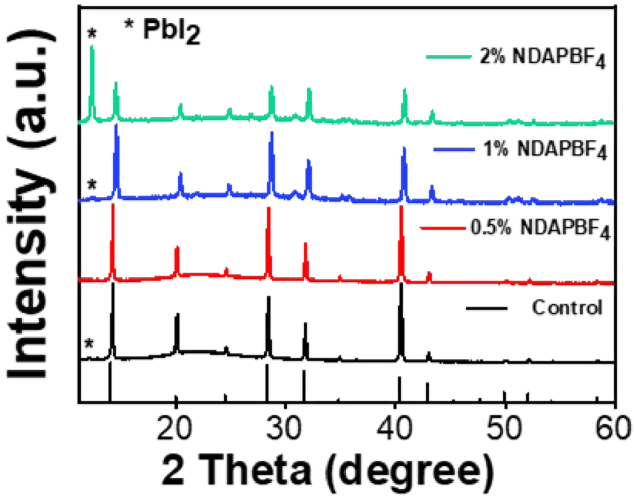

Figure S3 XRD patterns for $NDAPBF_4$ concentration from 0% - 2%

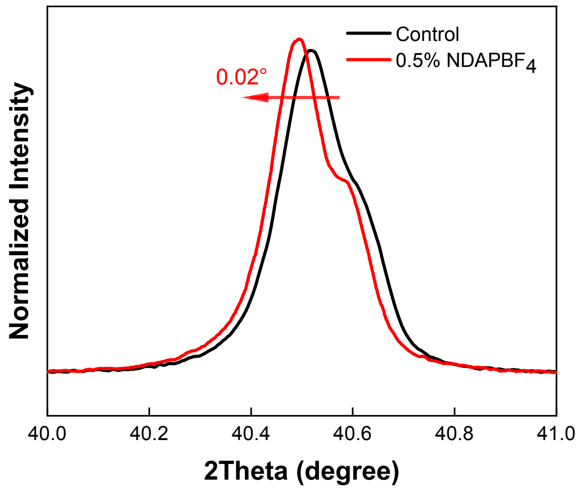

Figure S4 XRD patterns from 40° to 41°

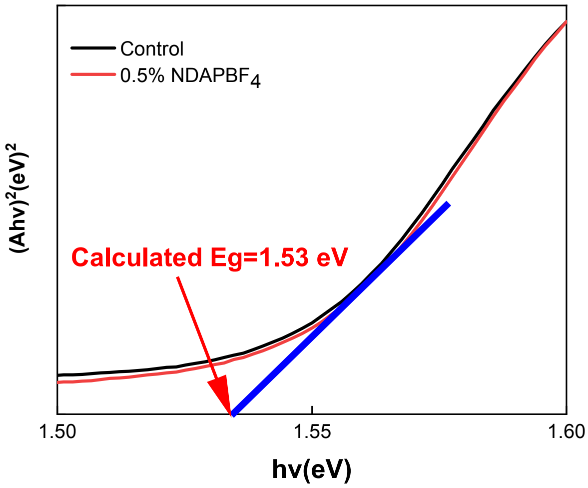

Figure S5. Tauc plot of perovskite films

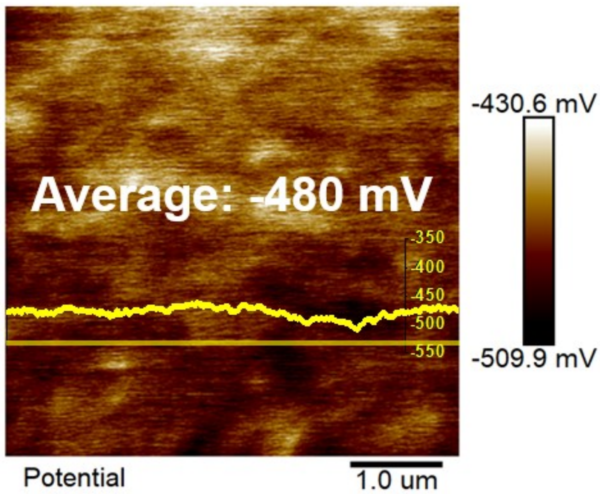

Figure S6. KPFM images of control films

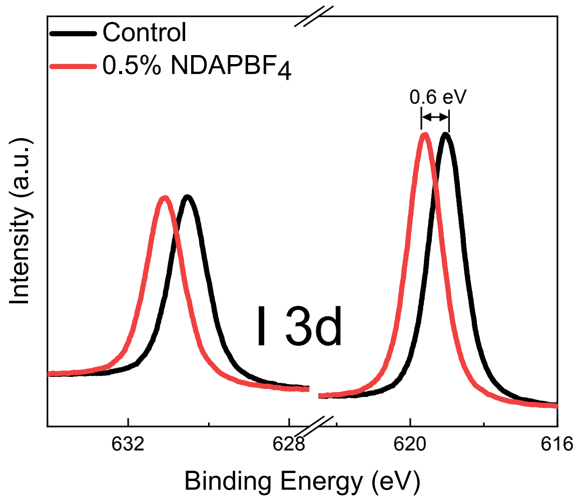

Figure S7 XPS spectra of I 3d.

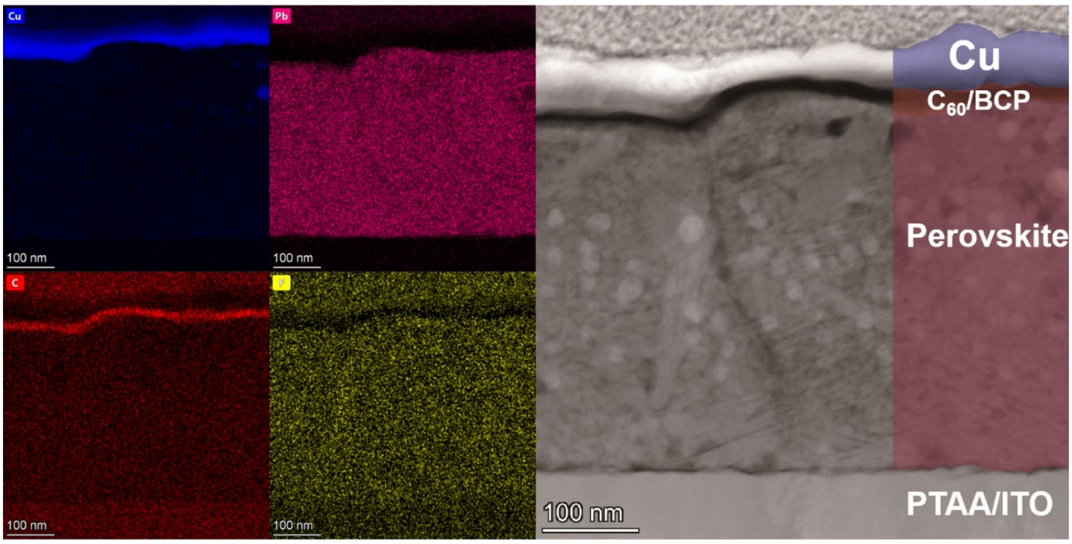

Figure S8 EDS mapping and TEM spectra of 0.5% $NDAPBF_4$ device

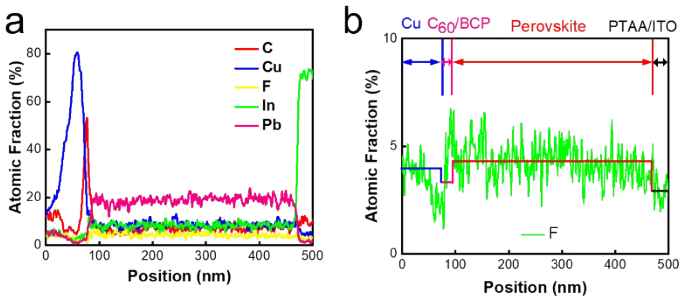

Figure S9 a) Element distribution derived for EDS mapping of 0.5% $NDAPBF_4$ device b) Element distribution of F

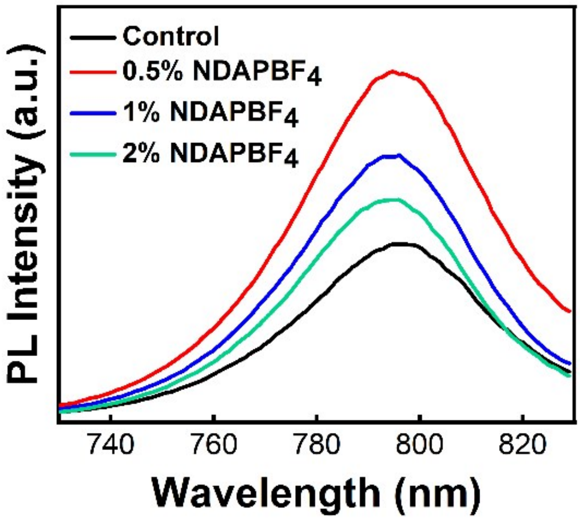

Figure S10 PL spectra for $NDAPBF_4$ concentration from 0% to 2%

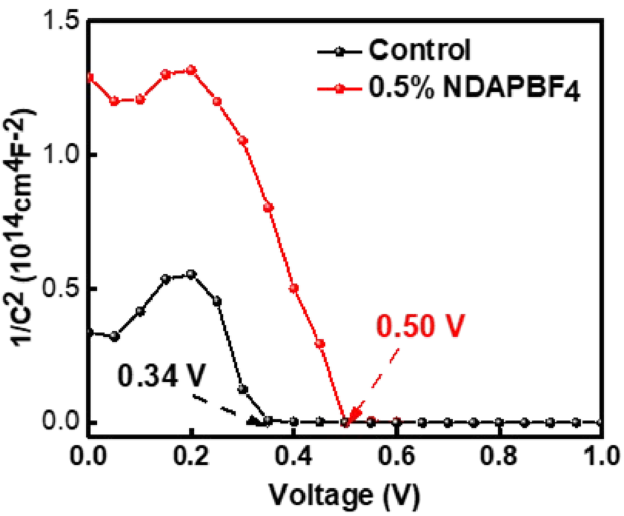

Figure S11 Mott-Schottky plots for control and 0.5% $NDAPBF_4$ devices

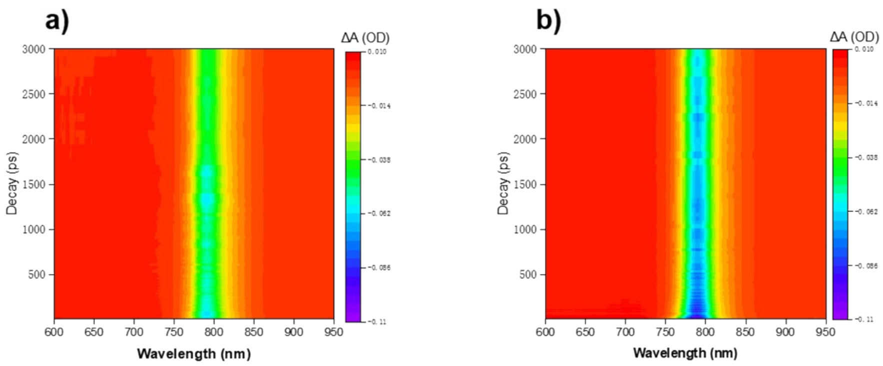

Figure S12. a-b) Pseudo-color maps of control (a) and $NDAPBF_4$ treated (b) films derived by TA

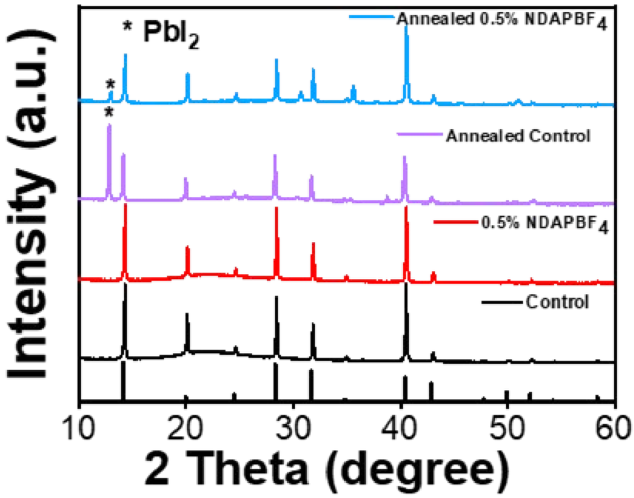

Figure S13 XRD before and annealed at 250℃ 3 min for control and 0.5% $NDAPBF_4$ devices

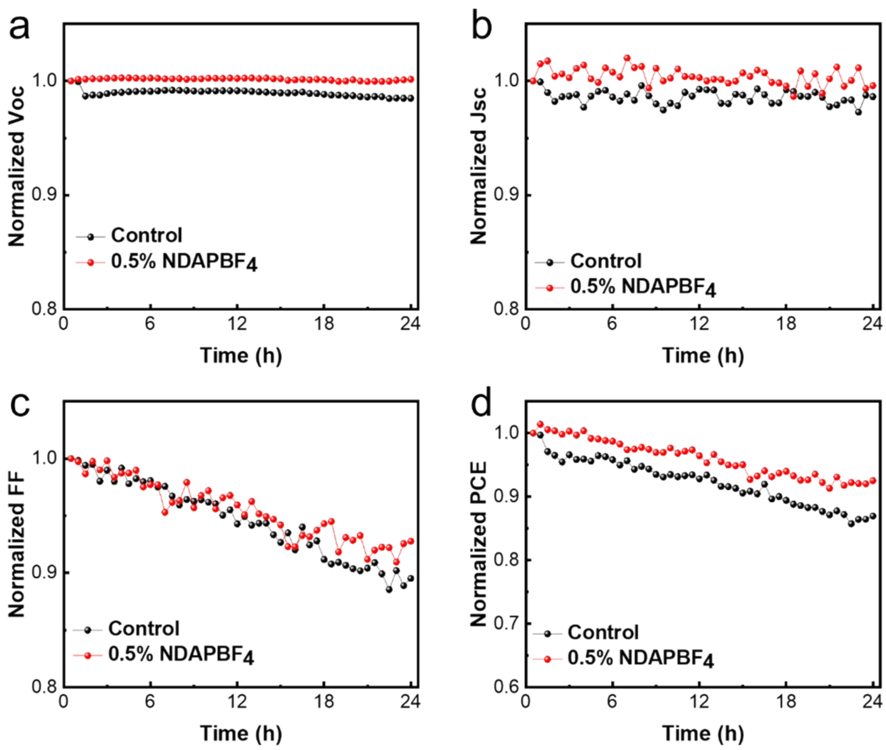

Figure S14 Operation stability of a) Voc b)Jsc c)FF d)PCE for control and 0.5% $NDAPBF_4$ devices

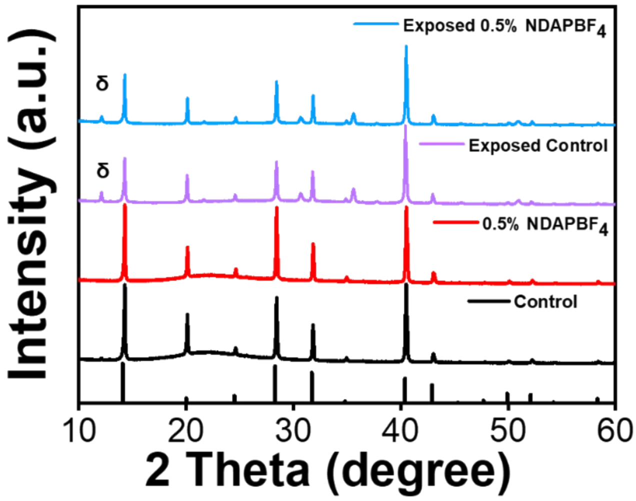

Figure S15 XRD before and after exposing to 60%-75% humidity for 24h for control and 0.5% $NDAPBF_4$ devices

Reference:

(1) Stolterfoht, M.; Wolff, C. M.; Márquez, J. A.; Zhang, S.; Hages, C. J.; Rothhardt, D.; Albrecht, S.; Burn, P. L.; Meredith, P.; Unold, T.; Neher, D. Visualization and suppression of interfacial recombination for high-efficiency large-area pin perovskite solar cells. *Nature Energy* **2018,** *3* (10), 847-854, DOI: 10.1038/s41560-018-0219-8.

(2) Thote, A.; Jeon, I.; Lee, J.-W.; Seo, S.; Lin, H.-S.; Yang, Y.; Daiguji, H.; Maruyama, S.; Matsuo, Y. Stable and Reproducible 2D/3D Formamidinium–Lead–Iodide Perovskite Solar Cells. *ACS Applied Energy Materials* **2019,** *2* (4), 2486-2493, DOI: 10.1021/acsaem.8b01964.

(3) Brinkmann, K. O.; He, J.; Schubert, F.; Malerczyk, J.; Kreusel, C.; van Gen Hassend, F.; Weber, S.; Song, J.; Qu, J.; Riedl, T. Extremely Robust Gas-Quenching Deposition of Halide Perovskites on Top of Hydrophobic Hole Transport Materials for Inverted (p-i-n) Solar Cells by Targeting the Precursor Wetting Issue. *ACS Appl Mater Interfaces* **2019,** *11* (43), 40172-40179, DOI: 10.1021/acsami.9b15867.

(4) Chen, Y.; Yang, Z.; Jia, X.; Wu, Y.; Yuan, N.; Ding, J.; Zhang, W.-H.; Liu, S. Thermally stable methylammonium-free inverted perovskite solar cells with Zn2+ doped CuGaO2 as efficient mesoporous hole-transporting layer. *Nano Energy* **2019,** *61*, 148-157, DOI: 10.1016/j.nanoen.2019.04.042.

(5) Zhu, H.; Wu, S.; Yao, J.; Chen, R.; Pan, M.; Chen, W.; Zhou, J.; Zhang, W.; Wang, T.; Chen, W. An effective surface modification strategy with high reproducibility for simultaneously improving efficiency and stability of inverted MA-free perovskite solar cells. *Journal of Materials Chemistry A* **2019,** *7* (37), 21476-21487, DOI: 10.1039/c9ta07238a.

(6) Wang, H.; Song, Y.; Kang, Y.; Dang, S.; Feng, J.; Dong, Q. Reducing photovoltage loss at the anode contact of methylammonium-free inverted perovskite solar cells by conjugated polyelectrolyte doping. *Journal of Materials Chemistry A* **2020,** *8* (15), 7309-7316, DOI: 10.1039/d0ta00892c.

(7) Li, S.; Fan, K.; Cui, Y.; Leng, S.; Ying, Y.; Zou, W.; Liu, Z.; Li, C.-Z.; Yao, K.; Huang, H. Unravelling the Mechanism of Ionic Fullerene Passivation for Efficient and Stable Methylammonium-Free Perovskite Solar Cells. *ACS Energy Letters* **2020,** *5* (6), 2015-2022, DOI: 10.1021/acsenergylett.0c00871.

(8) Lin, Y. H.; Sakai, N.; Da, P.; Wu, J.; Sansom, H. C.; Ramadan, A. J.; Mahesh, S.; Liu, J.; Oliver, R. D. J.; Lim, J.; Aspitarte, L.; Sharma, K.; Madhu, P. K.; Morales-Vilches, A. B.; Nayak, P. K.; Bai, S.; Gao, F.; Grovenor, C. R. M.; Johnston, M. B.; Labram, J. G.; Durrant, J. R.; Ball, J. M.; Wenger, B.; Stannowski, B.; Snaith, H. J. A piperidinium salt stabilizes efficient metal-halide perovskite solar cells. *Science* **2020,** *369* (6499), 96-102, DOI: 10.1126/science.aba1628.

(9) Peng, Z.; Wei, Q.; Chen, H.; Liu, Y.; Wang, F.; Jiang, X.; Liu, W.; Zhou, W.; Ling, S.; Ning, Z. Cs0.15FA0.85PbI3/CsxFA1-xPbI3 Core/Shell Heterostructure for Highly Stable and Efficient Perovskite Solar Cells. *Cell Reports Physical Science* **2020,** *1* (10), DOI: 10.1016/j.xcrp.2020.100224.